Neurobiology of Disease 213 (2025) 107019

Contents lists available at ScienceDirect

Neurobiology of Disease

journal homepage: www.elsevier.com/locate/ynbdi

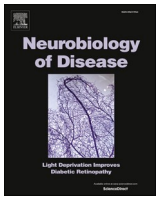

Increased BNIP3-mediated mitophagy attenuates GDAP1 loss of function - implications for Charcot-Marie-Tooth disease 4A

Li Zhang [a,1], Alireza Pouya [a,1], Janina Kopetzky [a,1], Sara Bitar [a], Christina Wolf [a], Federica Dal Bello [a], David Gomez-Zepeda [b,c,d], Stefan Tenzer [b,c,d], Axel Methner [a,*]

[a] Institute of Molecular Medicine, University Medical Center Mainz, Germany
[b] Institute for Immunology, University Medical Center Mainz, Germany
[c] Helmholtz Institute for Translational Oncology Mainz (HI-TRON Mainz) - A Helmholtz Institute of the DKFZ, Mainz, Germany
[d] German Cancer Research Center (DKFZ) Heidelberg, Heidelberg, Germany

ARTICLE INFO

Keywords:
Charcot-Marie-tooth (CMT) disease
GDAP1
Mitophagy
BNIP3
Drosophila

ABSTRACT

Charcot-Marie-Tooth disease type 4 A ((CMT4A), an autosomal recessive neuropathy, is caused by mutations in ganglioside-induced differentiation-associated protein 1 (*GDAP1*). GDAP1 resides in the outer mitochondrial membrane facing the cytosol and is involved in mitochondrial dynamics and function. Its perturbation affects mitochondrial shape, contact sites, redox homeostasis and cellular metabolism. In response to *GDAP1* knockdown in a human neuronal cell line, we found increased mitochondrial turnover, biogenesis and mitophagy. This was associated with more lysosomal proteins in mitochondrial fractions including BCL2/adenovirus E1B 19 kDa protein-interacting protein 3 (BNIP3) and its homolog BNIP3-like (BNIP3L) – proteins involved in the recruitment of autophagy machinery via direct interaction. Flies with neural *Gdap1* knockdown also exhibited upregulated levels of the sole BNIP3 ortholog. Neural expression of human BNIP3 reduced the detrimental effects of *Gdap1* knockdown on eclosion and climbing ability in adult flies, while simultaneous knockdown of both genes was detrimental. These findings suggest that increased BNIP3-driven mitophagy may act as a protective mechanism, partially counteracting the cellular dysfunction caused by *GDAP1* loss of function, and highlight the potential of targeting mitophagy pathways as a therapeutic strategy for CMT4A.

1. Introduction

Charcot-Marie-Tooth (CMT) disease represents the most commonly inherited form of peripheral neuropathy worldwide, affecting approximately one in every 2500 individuals. This collective group of disorders is characterized by its diversity in inheritance patterns, onset ages, and distinct electrophysiological features that help differentiate between demyelinating and axonal types. Notably, mutations in the *GDAP1* gene (encoding the ganglioside-induced differentiation-associated protein 1) are responsible for various forms of CMT. Among these, the most prevalent is the recessively inherited demyelinating subtype, CMT4A (Baxter et al., 2002), the axonal-recessive (AR)-CMT2 (Cuesta et al., 2002), the intermediate-recessive subtype CMTRIA (Senderek et al., 2003), and the dominant subtype CMT2K (Chung et al., 2008).

One potential mechanism of GDAP1 action that has been connected to CMT4A disease is mitochondrial dynamics. GDAP1 is located in the mitochondrial outer membrane facing the cytosol and overexpression of wildtype *GDAP1*, but not overexpression of *GDAP1* bearing recessive disease-causing mutations, results in more fragmented mitochondria, whereas *GDAP1* knockdown (KD) results in mitochondrial elongation (Niemann et al., 2005). This GDAP1-mediated mitochondrial fragmentation depends on the activity of dynamin-related protein 1 (DRP1), the major mitochondrial fission factor (Huber et al., 2013; Niemann et al., 2009). We recently demonstrated that *GDAP1* loss of function restricts the access of DRP1 to mitochondria by affecting the actin cytoskeleton (Wolf et al., 2022). We also found that *GDAP1* deficiency disrupts mitochondria-endoplasmic reticulum (ER) contact sites, leading to reduced mitochondrial Ca^{2+} levels and inhibition of the pyruvate dehydrogenase complex. These alterations result in a shift toward glutamine and fatty acid metabolism to compensate for the impaired Krebs' cycle. The findings from this study provided a mechanistic link between the actin cytoskeleton, mitochondrial dynamics, Ca^{2+} homeostasis, and

* Corresponding author at: Johannes Gutenberg University Medical Center Mainz, Institute for Molecular Medicine, Langenbeckstr. 1, D-55131 Mainz, Germany.
E-mail address: axel.methner@gmail.com (A. Methner).
[1] These authors contributed equally to this work.

https://doi.org/10.1016/j.nbd.2025.107019
Received 11 February 2025; Received in revised form 3 July 2025; Accepted 3 July 2025
Available online 4 July 2025

metabolic rewiring in the pathogenesis of CMT4A (Wolf et al., 2022). Interestingly, a pathogenic mutation of pyruvate dehydrogenase kinase isoenzyme 3 (PDK3) that inhibits the pyruvate dehydrogenase complex (PDC) also causes CMT disease, CMTX6 (Kennerson et al., 2013), making this a likely cause of CMT4A.

However, GDAP1 also remotely resembles glutathione-S-transferases, enzymes involved in detoxification. The catalytic activity of GDAP1 is still a matter of ongoing debate (Googins et al., 2020; Huber et al., 2016; Pedrola et al., 2005; Shield et al., 2006). In line with these structural features, GDAP1 perturbation has been found to affect the cellular redox homeostasis; *GDAP1* overexpression in neuronal cells increased cellular glutathione (GSH) content and protected against oxidative distress induced by GSH depletion. In contrast, *GDAP1* KD or expression of CMT-associated *GDAP1* mutants reduced GSH levels and increased susceptibility to oxidative distress (Noack et al., 2012). These findings implicate oxidative distress in the pathogenesis of CMT4A.

As a third potential mechanism, recent research demonstrated that GDAP1 is involved in basal autophagy and early autophagic processes by interacting with proteins crucial for autophagosome biogenesis and membrane trafficking, including Syntaxin 17 (a protein involved in autophagosome maturation) and LC3 (microtubule-associated protein 1 A/1B-light chain 3) (Cantarero et al., 2021). GDAP1 depletion led to autophagosome accumulation, reduced autophagic flux, and enlarged lysosomes with intact hydrolytic activity but impaired autophagic lysosome reformation. GDAP1 and Lysosome-Associated Membrane Protein 1 (LAMP1) were identified as a tethering pair for mitochondria-lysosome contact sites, which were accordingly significantly reduced in *GDAP1*-deficient cells. Co-immunoprecipitation studies have also demonstrated direct interactions between GDAP1 and Beclin-1, a key regulator of autophagy initiation (Cantarero et al., 2021). While glutathione supplementation restored lysosomal morphology and mitochondrial defects, it did not rescue early autophagic events or mitochondria-lysosome contacts, suggesting that GDAP1's function in these processes extends beyond its role in oxidative distress regulation (Cantarero et al., 2021). Together, these results implied a role for mitophagy, a selective form of autophagy that eliminates damaged or dysfunctional mitochondria, in the pathogenesis of CMT4A. Different mitophagy pathways exist: The PINK1 (PTEN induced kinase 1) and Parkin pathway is activated by mitochondrial depolarization, leading to Parkin-mediated ubiquitination of mitochondrial proteins and subsequent mitophagy. BNIP3 (BCL2/adenovirus E1B 19 kDa protein-interacting protein 3) and BNIP3L (BNIP3-like), on the other hand, are mitochondrial outer membrane proteins that directly interact with LC3 (which apparently also interacts with GDAP1 (Cantarero et al., 2021)), on autophagosomes, promoting mitophagy under conditions of hypoxia or oxidative distress. These diverse pathways ensure efficient removal of damaged mitochondria to maintain cellular health (recently reviewed in (Vargas et al., 2023)).

It would obviously be advantageous to have an in vivo model for *GDAP1* loss of function but unfortunately, previous studies in mice are difficult to interpret. Niemann et al. observed no obvious phenotype up to an age of 13 months (Niemann et al., 2014), whereas Barneo-Muñoz et al. reported a very strong phenotype with progressive loss of peripheral motoneurons and defects in neuromuscular junctions starting at the age of three months (Barneo-Muñoz et al., 2015). Niemann et al. removed exon 5, which generates a truncated, non-functional protein, while Barneo-Muñoz et al. removed the start codon. Remnant expression of toxic N-terminally truncated *GDAP1* variants might cause the strong phenotype in the Barneo-Muñoz model. The mild phenotype in the Niemann model was, however, attributed to possible compensatory effects of the *GDAP1* homolog *GDAP1L1* (Niemann et al., 2014). Both mouse models of *GDAP1* deficiency are therefore not ideal. Fortunately, the *Drosophila melanogaster* genome encodes only one GDAP1-like protein, *CG4623*, renamed *Gdap1* (López Del Amo et al., 2015). Perturbation of *Gdap1* by overexpression or RNAi-mediated KD produced alterations of mitochondrial size, distribution and morphology, oxidative distress, as well as neuronal and muscular degeneration (López Del Amo et al., 2015). Importantly, *Gdap1* KD could be rescued by human *GDAP1* showing that the function of GDAP1 is evolutionarily conserved. The same group later showed that both up- and down-regulation of *Gdap1* results in an early systemic inactivation of the insulin pathway before the onset of neuromuscular degeneration, followed by an accumulation of carbohydrates and an increase in the β-oxidation of lipids (López Del Amo et al., 2017), in line with our results in patient-derived motoneurons (Wolf et al., 2022). It therefore appears that, similar to studies of many other mitochondrial proteins (Debattisti and Scorrano, 2013), the fly is a suitable model to study the mechanism of action of GDAP1.

In this work, we found that *GDAP1* KD in human neuronal cells increases mitochondrial turnover, biogenesis, and mitophagy mediated by BNIP3 and BNIP3L. In Drosophila, neural-specific *Gdap1* KD impairs eclosion, climbing ability, and lifespan, with upregulated *BNIP3* ortholog levels. Overexpressing human *BNIP3* in Gdap1 KD flies attenuates these defects, while simultaneous KD exacerbates them. These findings suggest increased BNIP3-driven mitophagy may partially mitigate cellular dysfunction caused by GDAP1 loss. Our study further establishes the fruit fly as a valuable CMT4A model and highlights the complex interplay between mitochondrial dynamics, quality control, and cellular dysfunction in CMT4A pathogenesis.

2. Material and methods

2.1. Immunoblotting

Denatured total cellular protein samples were separated on SDS polyacrylamide gels 4–15% Mini-PROTEAN® TGX Stain-Free™ gels (Bio-Rad) and transferred onto a nitrocellulose membrane using the Trans-Blot® Turbo™ Transfer System (Bio-Rad). Membranes were blocked with 3% (*w/v*) milk powder in TBS-T (TBS, 0.05% (*v*/v) Tween 20) for 1 h (h) at room temperature (RT), blots stained with BNIP3L were blocked with 5% BSA in TBS-T. Chameleon Duo Pre-stained Protein Ladder (Li-Cor Biosciences) was used as a molecular weight standard. Primary antibodies were anti-actin mAB (clone C4, 1:2000, Millipore, MAB1501), anti-GDAP1 (1:750, Sigma HPA014266), anti-ATP5a (1:1000, Thermo Scientific, 439,800), anti-BNIP3 (1:1000, Cell Signaling Technology, 44060S), anti-BNIP3L (1:1000, Cell Signaling, D4R4B). The membranes were incubated with the primary antibodies overnight at 4 °C. For visualization, membranes were incubated with IRDye 800-conjugated anti-rabbit, or 680-conjugated anti-mouse IgG secondary antibody (1:10,000; Licor), for 1 h at RT and detected with the Odyssey Infrared Imaging System (Licor). Western Blots were analyzed with the Image Studio Lite Software (Li-Cor Biosciences).

2.2. Fly work

Fly strains: The fly stocks used in this paper are from the Bloomington Drosophila Stock Center (BDSC), including UAS-*Gdap1*-RNAi (BDSC 51903), *elav*-GAL4 (BDSC 458), UAS-*Bnip3*-RNAi (BDSC 42494), and the control line UAS-*mito.HA.GFP* (BDSC 8442), and from the Vienna Drosophila Resource Center (VDRC), including the RNAi control strain UAS-*always-early*-RNAi (VDRC 13673). The UAS-*hBNIP3*-HA/GFP, CyO line was a kind gift from Alex Whitworth (Mitochondrial Biology Unit, MRC, Cambridge, UK). Lifespan: Fruit flies were maintained on standard molasses-based food in a climate-controlled chamber set at 25 °C with a 12-h light/dark cycle. Food was replaced every two days, and mortality was recorded. Each experiment included at least four groups, each with approximately 25 flies. Climbing Assay: For each genotype and age, a minimum of four groups with roughly 25 flies per group were tested in vials with a 2 cm diameter. The percentage of flies able to climb either 8 cm or 6 cm within 8 s or 6 s (as specified) was recorded. The assay was consistently conducted at the same time of day. Eclosion Scoring: For each cross, 10 virgin female flies and 5 male flies

(2 days old) were paired as parents, with at least three replicates per condition. Parent flies were removed after four days, and the number of eclosed flies was recorded up to 14 days post-crossing. Quantitative RT-PCR: Total RNA was extracted using the ZR RNA MiniPrep kit (Zymo Research), and cDNA was synthesized from 10 ng/μL RNA using the High Capacity cDNA Reverse Transcription Kit (Life Technologies). For qPCR, FastStart Universal SYBR Green Master (Rox) (Merck) was used, with primers from Eurofins available upon request. Transcriptional levels were calculated using the $2-\Delta\Delta Ct$ method, where $\Delta\Delta Ct = \Delta Ct$ of the experimental group – mean ΔCt of control groups, and $\Delta Ct = Ct$ (gene of interest) – Ct (RpL32/Rp49). RpL32/Rp49 was used as the housekeeping control. Only male flies were used for these experiments. Primer sequences are as follows: *dmrp49*: F 5′-FCGGATCGATATGCTAAGCTGT-3′, R 5′-GCGCTTGTTCGATCCGTA-3′; *dmGdap1*: F 5′-TACAACTTCCATGCGCAAAA-3′, R 5′-GGTCCACCACATAGGGAAAG-3′; *dmBnip3*: F 5′-CACCAAAATCGAGCGAAGA-3′, R 5′-GCAGCTGTTGTGCTGAGTTC-3′ *hsBNIP3*: F 5′-CAGCCGAAAACGGCTCAAAA-3′, R 5′-TGTTTGGTGGGTTTGGGGAG-3′; *hsBNIP3L*: F 5′-ACATCACCATCATCAAAGACC-3′, R 5′-TCGTCAAAATCATTCTCCATCC-3′; *hsACTB*: F 5′-GTTGTCGACGACGAGCG-3′, R 5′-GCACAGAGCCTCGCCT-3′ (*Drosophila melanogaster, dm*; *Homo sapiens, hs*).

2.3. Dual-Glo® Luciferase assay

Cells were seeded in 96-well plates. Next day, cells were co-transfected with Firefly luciferase construct under expression control of the PGC1α promoter (addgene 8887) and Renilla luciferase construct under control of CAG promoter as a control. After 2 days, the luciferase activity was assessed by the Dual-Glo® Luciferase Assay System (Promega, E2920) according to the manufacturer's instructions. The Dual-Glo® Reagent equal to the volume of culture medium (75 μL) was added to each well and mixed and incubated for 15 min (min). The firefly luminescence was determined with a microplate reader (Tecan infinite 200Pro) in luminescence mode (6 kinetic cycles and 10,000 milliseconds integration time for each well). Then, the Dual-Glo® Stop & Glo® Reagent equal to the original culture medium volume (75 μL) was added to each well and mixed and incubated for an extra 15 min. The Renilla luminescence was measured in the same plate order and the same method as the firefly luminescence. The luminescence averages of 6 times reads were calculated, and the *PGC1α* promoter derived luminescence (Firefly) normalized to luminescence from the control (Renilla). Then, the relative ratio between cell lines was calculated from the normalized ratios.

2.4. Real-time PCR in GDAP1-KD SH-SY5Y cells

Quantitative real-time PCR was done with a 7500 real-time PCR system (Applied Biosystems), TaqMan Gene Expression Master Mix (Roche) and 5′-FAM-labelled probes of the Universal Probe Library (Roche). The primers utilized in this study: *GDAP1* (tgttttagatggtgcctgtgag – ctcccactgactggacatga), *PGC1α* (tgagagggccaagcaaag – ataaatcacacggcgctctt), *PGC1b* (agtcaacggccttgtgttaag – acaacttcggctctgagactg), TFB2M (aatttgggaatagaagcagttcc - acttgggaacattccaactacttt). Relative gene expression was calculated by 2-ΔΔCt compared to the *HPRT* gene.

2.5. Genetically-encoded indicators

Genetically encoded recombinant proteins were utilized which indicate cellular components or physiological properties. Cells were transfected with the indicators, and after 2 days, the fluorescence intensities were captured in transfected cells by an inverted TCS-SP5 confocal microscope (Leica) with appropriate excited/emission wavelengths. Grx1-roGFP2 indicator (Gutscher et al., 2008) was used to measure cytoplasmic GSSG/GSH ratio. The ratio of green fluorescent (520 nm) emitted with 405 per the same channel signals when emitted with 476 nm corresponds to the GSSG/GSH ratio. Mito-Timer reporter gene encodes a mitochondrial targeted green fluorescence protein which shifts irreversibly to red fluorescence when oxidized (Laker et al., 2014). The fluorescence intensities of Mito-Timer analyzed at following excited/emission wavelengths, 488/518 nm, and 561/572 nm. The red/green fluorescence intensity represents the amount of oxidized form of Mito-Timer. Mito-Keima is a mitochondrial-targeted probe that indicates mitophagy. The excitation spectra of the probe are pH-dependent, with the excitation peak ratio of Keima (550/438) increasing at acidic pHs. The fluorescence intensity ratio at 620 nm (F550/F438) reflects an acidic environment, and an increase in this ratio indicates that mitochondria are being delivered to lysosomes to undergo mitophagy (Katayama et al., 2011).

2.6. Cell culture and generation of stable cell lines

SH-SY5Y cell lines were grown in DMEM/F12 medium (Gibco) supplemented with 10 % (*v*/v) fetal calf serum (FCS; Thermo Scientific), 2 mM L-glutamine (Gibco), 1× MEM non-essential amino-acids, 100 U/ml penicillin and 100 μg/ml streptomycin (Gibco) in a humidified incubator at 37 °C, 5% CO_2 and 95% air. The SH-SY5Y cell lines pLKO-NT (control) and G4 (knockdown) were a kind gift of David Pla-Martin and Francesc Palau (Pla-Martín et al., 2013) and were grown in growth medium containing 2 μg/mL puromycin (InvivoGen).

2.7. Protein extraction and digestion

The method for crude mitochondria isolation was adapted from Wieckowski's protocol (Wieckowski et al., 2009). Cells were harvested, washed once with cold PBS, and resuspended in 10 mL of mitochondrial isolation buffer 1 (containing 225 mM D-mannitol, 75 mM sucrose, 30 mM Tris-HCl, 0.1 mM EGTA; 1× protease inhibitor cocktail). Cells were disrupted using a nitrogenase cavitation chamber at a pressure of 60 bar for 10 min. Afterwards, the solution was centrifuged at 600*g* for 5 min twice to remove unbroken cells, nuclei and other residues. The supernatant containing mitochondria was collected and centrifuged at 7000*g* for 10 min. The crude mitochondrial pellet was, then, resuspended in 1 mL Isolation Buffer 2 (containing 225 mM D-mannitol, 75 mM sucrose, 30 mM Tris-HCl; 1× protease inhibitor cocktail), centrifuged at 7000*g* for 5 min twice to remove membranes not associated with mitochondria, and finally resuspended in 1 mL mitochondrial isolation buffer (MRB, containing 250 mM D-Mannitol, 5 mM HEPES, 0.5 mM EGTA). The protein concentration of the crude mitochondrial fraction was determined and 10 μg were used for the MS analysis. During the whole procedure, solutions were kept on ice and all centrifugation steps performed at 4 °C. Proteins were lysed in 5 μL of lysis buffer (10% SDS in 50 mM HEPES with Complete Protease Inhibitor Cocktail-EDTA) assisted by sonication in a Bioruptor system (Diagenode) for 15 min in cycles of 30 s (s) on, 30 s off. Protein samples were digested using the "Single-Pot Solid-Phase-Enhanced Sample Preparation" (SP3) protocol with modifications (Hughes et al., 2014; Sielaff et al., 2017) as previously described (Wolf et al., 2022). Proteins were reduced by adding 5 μL of 200 mM Dithiothreitol (DTT) per 100 μL lysate and incubating samples for 30 min at 45 °C. Then, proteins were alkylated by adding 10 μL 100 mM Iodoacetamide (IAA) per 100 μL lysate and incubating for 30 min at RT in the dark. To quench the IAA, 10 μL 200 mM DTT were added per 100 μL lysate. Magnetic carboxylate modified particles Beads (SpeedBeads, Sigma) were added, and proteins were bound to them by adding acetonitrile (ACN) to a final concentration of 70% and incubating for 18 min at RT. Magnetic beads were captured by placing the tubes on a magnetic stand for 2 min. Then, the supernatant was removed, and the beads were washed twice with 70% ethanol (EtOH) and once with ACN. Proteins were digested by adding 5 μL digestion buffer with trypsin (50 mM ammonium bicarbonate, 1:25 *w*/w trypsin: protein ratio) and incubating overnight at 37 °C. The resulting peptides were washed twice with ACN at a final concentration of 95%. Peptides

were eluted in 10 µL 2% DMSO (in water) assisted by sonication in an ultrasonic bath for 1 min and the supernatant was recovered after centrifugation. Finally, 10 µL of the resulting supernatant were mixed with 5 µL 100 fmol/µL Enolase digest (Waters Corporation), acidified with 5 µL 1% formic acid (FA), and transferred to LC-MS vials.

2.8. Liquid chromatography-mass spectrometry (LC-MS) analysis

Tryptic peptides were analyzed by LC-MS on a NanoAQUITY UPLC system coupled with a Synapt G2-Si (Waters Corporation). Peptides were directly injected and separated in a 75 µM × 250 mm HSS-T3 C18 column (Waters Corporation) heated to 55 °C. *mobile* phase A was composed of 0.1% (*v*/v) formic acid (FA) and 3% (v/v) DMSO in water. Mobile phase B was composed of 0.1% (v/v) FA and 3% (v/v) DMSO in ACN. Peptides were separated in a 90 min chromatographic gradient from 5 to 40% (v/v) mobile phase B at a 300 nL/ min flow rate. MS analysis of eluting peptides was performed by ion-mobility enhanced data-independent acquisition (UDMS^E) (Distler et al., 2014). Precursor ions (MS) were collected in low-energy mode at a constant collision energy of 4 eV. Fragment ions (MS/MS) were acquired in the elevated energy scan applying drift-time specific collision energies. The spectral scan time was 0.6 for the low-energy (MS) and 1.0 s for the high-energy (MS/MS) modes. [Glu1]-fibrinopeptide (100 fmol/µL) was constantly infused via the reference sprayer of the NanoLockSpray source and data were acquired every 30 s as lock mass reference.

2.9. Data processing and label-free protein quantification

LC-MS UDMS^E data was processed using ProteinLynx Global Server (PLGS, ver. 3.0.2, Waters Corporation). The resulting proteins were searched against the human UniProt proteome database (*Homo sapiens*, UniProtK-Swissprot release 2018_05) supplemented with a list of common contaminants. Database search was performed with the following settings, Trypsin as enzyme for digestion and peptides; up to two missed cleavages were allowed; carbamidomethylation on cysteine and oxidized methionine were set as fixed and variable modification, respectively. False discovery rate (FDR) assessment for peptide and protein identification were done using the target-decoy strategy and results were filtered at 1% FDR in PLGS. Retention time alignment, exact mass retention time (EMRT), as well as normalization and filtering were performed using ISOQuant (v.1.8) with TOP3 quantification using enolase as reference for calculating absolute in-sample amounts.

2.10. Statistical analysis

Normal distribution was tested using the D'Agostino-Pearson omnibus normality test. Statistical significance was then verified using appropriate parametric (Student's *t*-test or ANOVA) or non-parametric tests (Mann Whitney and Kruskal Wallis tests) followed by multiple comparison tests as indicated. Statistical analysis of mass spectrometry data was performed using two-tailed *t*-tests and subsequent Bonferroni-Hochberg correction, a $p < 0.05$ was considered to be statistically significant. Pathway over-representation analysis was performed using the STRING database with default parameters (Szklarczyk et al., 2020).

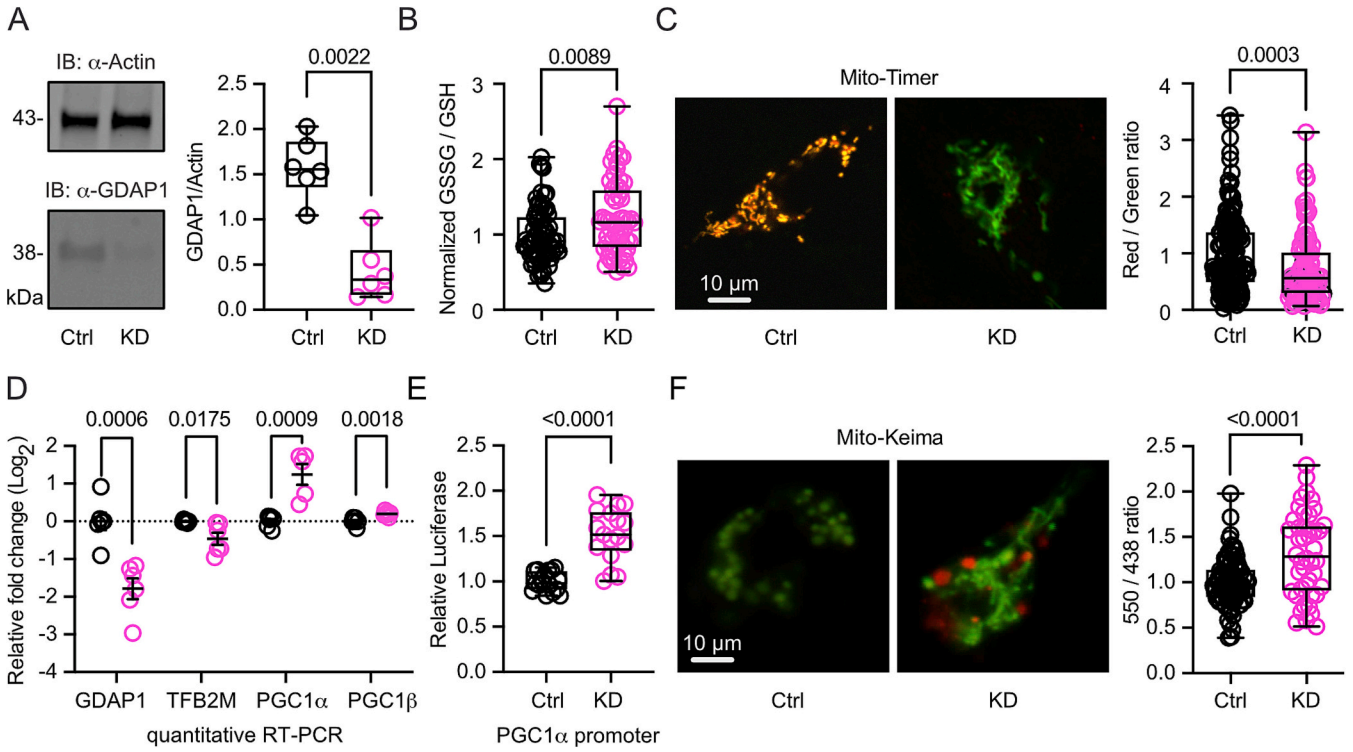

Fig. 1. Increased mitochondrial turnover and biogenesis in *GDAP1* knockdown cells. (A) Immunoblot analysis of control (Ctrl) and *GDAP1* knockdown (KD) SH-SY5Y cells showing successful *GDAP1* KD. Size is indicated, Actin served as loading control. (B) The normalized GSSG/GSH ratio was measured in *GDAP1*-KD and Ctrl cells expressing cytosolic Grx1-roGFP2 sensor. (C) Representative images show red/green fluorescence emitted from the Mito-Timer reporter on mitochondria in Ctrl and KD cells. The green color indicates younger mitochondria. The red/green ratio shown on the right represents the rate of mitochondrial age. (D) Quantitative RT-PCR analysis of *GDAP1*, *TFB2M*, *PGC1α*, and *PGC1β*. (E) Luciferase assay for *PGC1α* promoter activity, showing a significant increase in promoter activity in *GDAP1*-KD cells. (F) Mito-Keima fluorescence analysis in *GDAP1*-KD and Ctrl cells. The F550/F438 ratio reflects mitochondrial delivery to acidic lysosomes, with higher ratios indicating increased mitophagy. Statistical relevance was assessed by the Mann Whitney test in B and C, and unpaired *t*-tests in D, E and F. *P* values are indicated. (For interpretation of the references to colour in this figure legend, the reader is referred to the web version of this article.)

3. Results

3.1. Increased mitochondrial turnover and biogenesis in GDAP1 knockdown cells

GDAP1 knockdown (KD, Fig. 1A) in human neuronal SH-SY5Y cells (Pla-Martín et al., 2013) represents a suitable model system to study CMT4A, because changes observed in these cells closely mimic those observed in motoneurons differentiated from patient-induced induced pluripotent stem cells (Wolf et al., 2022). Based on previous studies (Cantarero et al., 2021; Noack et al., 2012) that reported an altered redox homeostasis in *GDAP1* loss of function models, we now studied the redox homeostasis in KD versus wildtype (WT) cells using the genetically-encoded Grx1-roGFP2 sensor (Gutscher et al., 2008) which quantifies the cytoplasmic GSSG/GSH ratio. This demonstrated a higher ratio of oxidized to reduced glutathione (GSSG/GSH) (Fig. 1B) and thus a more pro-oxidative environment, in line with previous work that demonstrated an increased susceptibility of *GDAP1* KD cells (Noack et al., 2012) and also KD flies (López Del Amo et al., 2015) to oxidative distress. We also used MitoTimer, a genetically-encoded dual emission fluorophore targeted to the mitochondrial matrix (Laker et al., 2014) to study the redox milieu within mitochondria. When newly synthesized, the mitoTimer protein emits green fluorescence. Over time, as the protein is exposed to the oxidative environment within mitochondria, it undergoes an irreversible chromophore maturation process that shifts the emission to red fluorescence. We were surprised to find a decreased red/green ratio and thus less oxidized mitochondria in *GDAP1* KD cells (Fig. 1C). Together with the increased pro-oxidative environment, we figured that this likely represents a shift to younger mitochondria, respectively increased mitochondrial turnover and evaluated the mRNA expression of key regulators of mitochondrial biogenesis: Transcription Factor B2, Mitochondrial (*TFB2M*), Peroxisome Proliferator-Activated Receptor Gamma Coactivator 1-alpha (*PGC1α*), and Peroxisome Proliferator-Activated Receptor Gamma Coactivator 1-beta (*PGC1β*). TFB2M is involved in mitochondrial transcription, whereas PGC1α and PGC1β are nuclear-encoded coactivators that enhance mitochondrial biogenesis by upregulating the expression of genes supporting mitochondrial function (Gleyzer et al., 2005; Litonin et al., 2010). In *GDAP1* KD cells, *TFB2M* was significantly downregulated, while *PGC1α* and *PGC1β* were upregulated (Fig. 1D). Dual luciferase assays demonstrated that the promoter region of *PGC1α* is more active in KD than in WT cells (Fig. 1E). We interpreted the findings of less oxidized, "younger" mitochondria, alongside reduced expression of the mitochondrial transcription factor TFB2M and increased nuclear transcription factors PGC1α and PGC1β, as indicative of mitochondrial DNA damage or a regulatory feedback mechanism from accumulated mitochondrial proteins. The upregulation of PGC1α and PGC1β and subsequent increased mitochondrial biogenesis likely reflects a compensatory response aimed at maintaining mitochondrial function under stress or dysfunction. Given the evidence for increased mitochondrial turnover and biogenesis in *GDAP1* KD cells, we hypothesized that this would be accompanied by enhanced removal of damaged or dysfunctional mitochondria through mitophagy. To test this, we employed mito-Keima, a genetically-encoded sensor that quantifies mitochondrial delivery to lysosomes. Mito-Keima fluorescence was used to assess mitophagy, where an increase in the F550/F438 ratio reflects the pH-dependent shift in excitation spectra as mitochondria transition from the neutral mitochondrial environment to acidic lysosomes for degradation (Katayama et al., 2011). This analysis confirmed our hypothesis, revealing significantly increased mitophagy in *GDAP1* KD cells (Fig. 1F).

3.2. Increased levels of lysosomal proteins and the mitophagy adaptor proteins BNIP3 and BNIP3L in mitochondrial fractions from GDAP1 knockdown cells

To better understand the molecular basis of the increased mitochondrial turnover and mitophagy observed in *GDAP1* KD cells, we next performed an unbiased proteomic analysis of crude mitochondrial fractions from KD and WT cells. This revealed quite substantial changes with 200 significantly upregulated proteins and 154 significantly downregulated proteins out of 3669 identified proteins as shown by a Volcano plot (Fig. 2A). Using STRING (Search Tool for the Retrieval of Interacting Genes/Proteins) analysis as a bioinformatics method to analyze and visualize protein-protein interaction networks, we found a quite substantial increase of lysosomal proteins among the upregulated proteins in addition to the mitochondrial proteins that were expected (Fig. 2B, permalink https://version-12-0.string-db.org/cgi/network?networkId=bdmcRvkFn7rQ). Lysosomal proteins were highly over-represented as shown by a Kyoto Encyclopedia of Genes and Genomes (KEGG) pathway enrichment analysis (Fig. 2C).

Of these, one protein specifically caught our attention because of its ability to connect mitochondria and lysosomes. The protein BNIP3 (highlighted in Fig. 2B) is located on the outer mitochondrial membrane and directly interacts with LC3 on autophagosomes thereby connecting these two organelles to selectively degrade damaged mitochondria. Quantitative RT-PCR and immunoblot analyses confirmed significant increases in BNIP3 and also of its homolog BNIP3L levels in mitochondrial fractions of GDAP1-KD cells compared to controls (Fig. 2D and E). Together with the increased mitochondrial turnover implied by the younger age of mitochondria in *GDAP1*-KD cells, this suggests that dysfunctional mitochondria are more rapidly removed in *GDAP1*-deficient cells by BNIP3/BNIP3L-mediated direct mitophagy.

3.3. Detrimental effect of neural Gdap1 knockdown in Drosophila melanogaster

To investigate whether increased BNIP3-mediated mitophagy is beneficial or detrimental on the organismal level, we next sought to establish an animal model for CMT4A. We chose *Drosophila melanogaster*, a proven in vivo model for *GDAP1* deficiency (López Del Amo et al., 2017; López Del Amo et al., 2015). Unlike mammals, which have both *GDAP1* and *GDAP1L1*, fruit flies only have one *GDAP1* homolog, reducing the likelihood of compensatory changes. We knocked down *Gdap1* in the nervous system using the UAS-GAL4 system with the neural-specific elav-GAL4 driver. Quantitative PCR analysis of fly heads confirmed effective *Gdap1* KD (Fig. 3A). *Gdap1* KD flies exhibited several detrimental effects. First, they had a reduced eclosion (emergence of adult flies from the pupal case) rate, suggesting that Gdap1 is essential for proper neural development and viability (Fig. 3B). This was slightly more pronounced in male flies. Second, in a climbing assay, young (2–7-day-old) male *Gdap1* KD flies had a significantly lower percentage able to climb above 8 cm within eight seconds compared to controls, indicating early motor impairment. This impairment was exacerbated with age, as 30-day-old *Gdap1* KD flies showed a near-complete loss of climbing ability (Fig. 3C). Finally, male *Gdap1* KD flies had a significantly shortened lifespan compared to controls (Fig. 3D). These findings — reduced eclosion rates, impaired motor function, and decreased lifespan — highlight the critical role of Gdap1 in maintaining neural function and survival in Drosophila. The Drosophila model thus provides a valuable platform to further investigate the mechanisms and consequences of altered BNIP3-mediated mitophagy in the context of *GDAP1* deficiency.

3.4. Upregulation of the fly BNIP3 ortholog in Gdap1 knockdown flies

To investigate the suitability of our model to study the effects of BNIP3 perturbation on *Gdap1* loss, we first aimed to replicate the findings obtained in human SH-SY5Y cells and examined *Bnip3* expression using quantitative PCR and immunoblotting in *Gdap1* KD flies. Importantly, similar to *GDAP1*, flies only contain one and not two *BNIP3* homologs, the fly ortholog is called *Bnip3* or *CG5059*. Quantitative PCR analysis confirmed an increase in *Bnip3* transcript levels in *Gdap1* KD

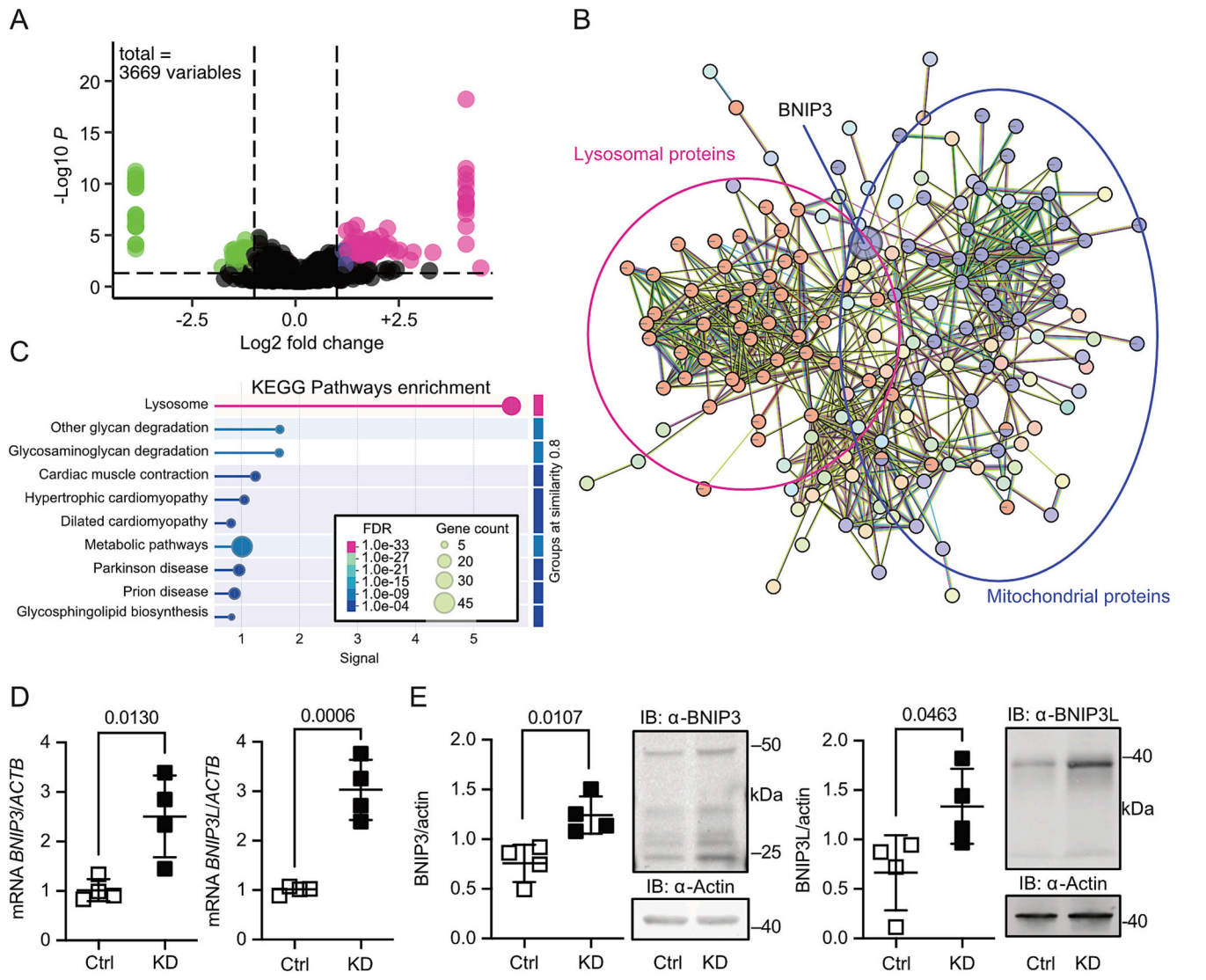

Fig. 2. Increased levels of lysosomal proteins and the mitophagy adaptor proteins BNIP3 and BNIP3L in mitochondrial fractions from GDAP1 knockdown cells. (A) Volcano plot of upregulated (magenta) and downregulated (green) proteins in mitochondrial fractions from *GDAP1* KD and control cells. (B) STRING and (C) KEGG pathway enrichment analyses of upregulated proteins demonstrates an increase in lysosomal proteins (magenta) in mitochondrial fractions from *GDAP1* KD cells (mitochondrial proteins in blue, other proteins in various colors). Mitochondrial proteins are shown in blue. (D) Quantitative RT-PCR in *GDAP1* knockdown (KD) and control (ctrl) cells. *ACTBN* served as housekeeping control. (E) Immunoblot analysis of BNIP3 and BNIP3L levels in mitochondrial fractions from Ctrl and KD cells, with quantification shown, confirming their upregulation in the KD group. Size is indicated, Actin served as loading control. Data in D and E show the results of 4 individual experiments, respectively, blots, statistical analysis was done using the student's *t*-test, *p* values are indicated. (For interpretation of the references to colour in this figure legend, the reader is referred to the web version of this article.)

flies driven by *elav*-GAL4 with UAS-*Gdap1*-RNAi, compared to controls (Fig. 4A). Immunoblot analysis further demonstrated significantly elevated Bnip3 protein levels in the heads of *Gdap1* KD flies, even if normalized to the mitochondrial protein Atp5a as a loading control (Fig. 4B). These findings suggest that *GDAP1* depletion results in a similar regulation of BNIP3 at the transcript and protein level in flies and man.

3.5. *BNIP3 protects against Gdap1 depletion*

The induction of BNIP3 by *Gdap1* KD allowed us to answer the question of whether this induction is detrimental or beneficial for *Gdap1* KD flies. Lifespan analysis (Fig. 5A) showed that concurrent KD of *Bnip3* and *Gdap1* (*elav* > *Gdap1*-RNAi, *Bnip3*-RNAi) significantly shortened lifespan compared to *Gdap1* or *Bnip3* KD alone, indicating that Bnip3 probably counteracts the negative effects of *Gdap1* depletion. In contrast, overexpression of human BNIP3 in *Gdap1* KD flies improved viability and motor function, as evidenced by the increased eclosion rate (Fig. 5B) and enhanced climbing ability in 30-day-old flies (Fig. 5C) compared to *Gdap1* KD flies. These results demonstrate that *BNIP3* overexpression can partially rescue the detrimental effects of *Gdap1* KD, implying a protective role for BNIP3 in maintaining neural function and survival under *Gdap1* depletion.

4. Discussion

In this study, we investigated the role of BNIP3 in the context of GDAP1 deficiency, a key factor in the pathogenesis of autosomal-recessive Charcot-Marie-Tooth disease type 4 A (CMT4A). We demonstrated that *GDAP1* knockdown in human neuronal cells leads to increased mitochondrial turnover and biogenesis, as well as elevated levels of mitophagy mediated by BNIP3 and BNIP3L. Furthermore, using a Drosophila model of CMT4A, we showed that neural-specific Gdap1 knockdown impairs eclosion, climbing ability, and lifespan,

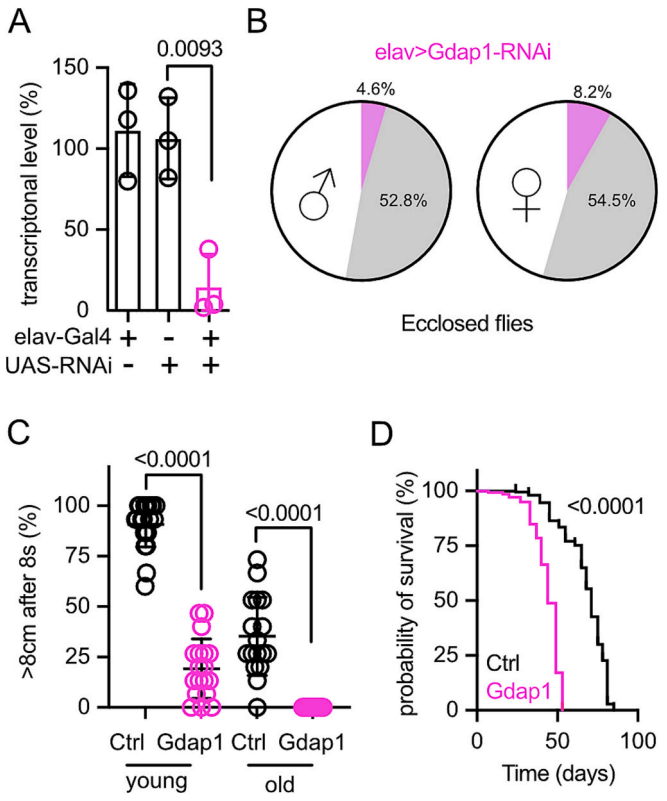

Fig. 3. Detrimental effect of neural Gdap1 knockdown in *Drosophila melanogaster*. (A) Quantitative PCR (qPCR) analysis of Gdap1 transcript levels in Drosophila neurons with neural-specific knockdown (KD) of Gdap1 driven by *elav*-GAL4 and UAS-*Gdap1*-RNAi. Controls include *elav*-GAL4 or UAS-RNAi alone. Each dot represents the mean value of triplicates from an RNA sample of eight heads. (B) Eclosion rate of *Gdap1* neural KD flies compared to controls, with pink indicating *elav* > *Gdap1*-RNAi flies and the other two colors (white and grey) representing non-*elav* > *Gdap1*-RNAi flies with a balancer chromosome. Male total 197 flies. Female total 195 flies. (C) Climbing ability assay for young (2–7 days) and old (30 days) flies, measuring the percentage able to climb above 8 cm within 8 s. Each dot represents one vial of approximately 25 flies. Ctrl is *elav* > *always-early* RNAi; Gdap1 is *elav* > *Gdap1*-RNAi. (D) Lifespan analysis of neural *Gdap1* KD flies (*elav* > *Gdap1*-RNAi) compared to control flies (*elav* > *always-early*-RNAi). Statistical significance was evaluated by one-way ANOVA followed by the Holm-Sidak multiple comparisons test in A and C, and the log-rank (Mantel-Cox) test in D. *P* values are indicated. (For interpretation of the references to colour in this figure legend, the reader is referred to the web version of this article.)

accompanied by upregulation of the sole *BNIP3* ortholog. Importantly, overexpression of human *BNIP3* in *Gdap1* knockdown flies attenuated these defects, while simultaneous knockdown of both genes exacerbated them suggesting a protective function of BNIP3 in CMT4A.

Our findings suggest that *GDAP1* deficiency leads to mitochondrial dysfunction, which triggers a compensatory increase in mitochondrial turnover and biogenesis. BNIP3 and BNIP3L are mitochondrial outer membrane proteins that are known to be induced under conditions of oxidative distress and hypoxia, promoting mitophagy to maintain mitochondrial quality control(Metukuri et al., 2009; Zhang and Ney, 2009). Consistent with this established function, we observed an abundance of lysosomal proteins and elevated levels of these mitophagy adaptor proteins BNIP3 and BNIP3L in crude mitochondrial fractions from *GDAP1* KD cells, suggesting that the increased mitochondrial turnover we observed is mediated by BNIP3-mediated mitophagy. The protective effect of BNIP3 overexpression in *Gdap1* knockdown flies supports the notion that enhanced BNIP3-mediated mitophagy can partially mitigate the cellular dysfunction caused by *GDAP1* loss. Multiple studies in Drosophila have demonstrated the protective role of

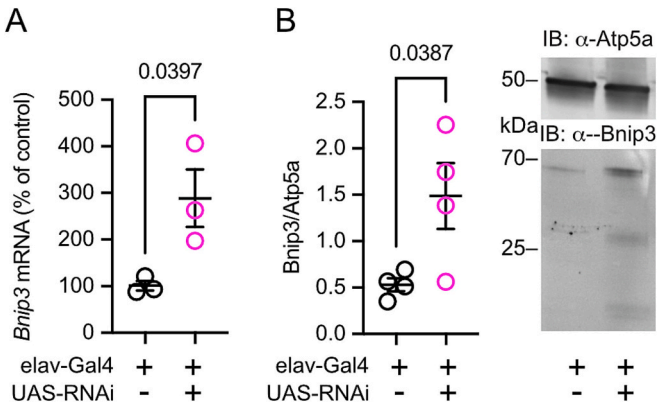

Fig. 4. Upregulation of the fly Bnip3 ortholog in Gdap1 knockdown flies. (A) Quantitative PCR analysis of Bnip3 transcript levels, normalized to Rp49, in the heads of Drosophila with neural-specific *Gdap1* knockdown (*elav*-GAL4 > *Gdap1*-RNAi). *Elav*-GAL4 alone was used as the control. Each dot represents the mean value of triplicate measurements from an RNA sample of eight fly heads. (B) Immunoblot analysis of Bnip3 protein levels, normalized to Atp5a as a loading control, in the heads of neural-specific Gdap1 knockdown flies, with *elav*-GAL4 alone as control. Each dot represents the mean value of triplicate measurements from a protein sample of eight fly heads. *P* values are indicated.

BNIP3-mediated mitophagy. In flies, neuronal induction of BNIP3-mediated mitophagy promotes mitochondrial quality control, enhances brain protection, and systemically slows aging, improving organismal health and longevity(Schmid et al., 2022; Zhang et al., 2016). *BNIP3* overexpression in the muscle tissue of *Pink1*-deficient flies restored mitochondrial morphology and ATP production while also rescuing phenotypic defects(Zhang et al., 2016), and BNIP3 facilitates mitochondrial DNA selection by promoting the elimination of damaged mitochondria(Lieber et al., 2019). Together, these findings establish a consistent pattern of BNIP3-mediated protection in Drosophila models of mitochondrial dysfunction.

While the protective role of BNIP3 is well-established in Drosophila, mammalian systems exhibit additional complexity due to alternative splicing of both BNIP3 and BNIP3L (recently reviewed in (Field and Gordon, 2022)). In mammalian cells, the full-length BNIP3 protein contains a transmembrane domain essential for its mitochondrial localization and pro-death function, while variants lacking this domain act as dominant-negative regulators that promote cell survival(Gang et al., 2011). Interestingly, pyruvate dehydrogenase kinase (PDK) activation—which we previously found elevated in GDAP1-deficient cells (Wolf et al., 2022)—has been shown to drive alternative splicing of BNIP3 toward cell survival variants(Gang et al., 2015). This suggests a potential mechanism by which GDAP1 deficiency might influence BNIP3 splicing patterns in favor of protective rather than cell death-promoting functions. This splicing-dependent balance between quality control and cell death pathways likely plays a critical role in determining neuronal fate in CMT4A pathogenesis.

GDAP1 has been reported to coordinate so-called mitochondria-lysosome contact sites by interacting with LAMP1 (Cantarero et al., 2021; Pijuan et al., 2022). *GDAP1* depletion in motoneurons and human neuroblastoma SH-SY5Y cells (Cantarero et al., 2021), or the expression of pathogenic variants such as W67L in patient-derived fibroblasts (Pijuan et al., 2022), results in the reduction of mitochondria-lysosome membrane contact sites. This reduction directly impacts lysosomal function, leading to lysosomal enlargement and disrupted autophagic flux well in line with our findings. This may be overcome by BNIP3 which can disrupt the Bcl-2/Beclin1 complex, freeing Beclin1 (an interactor of GDAP1 (Cantarero et al., 2021)) to initiate autophagy (Mazure and Pouysségur, 2009). It is of interest that other types of CMT have also been linked to mitophagy. Mutations in the mitofusin 2 (*MFN2*) gene, a key regulator of mitochondrial dynamics also involved

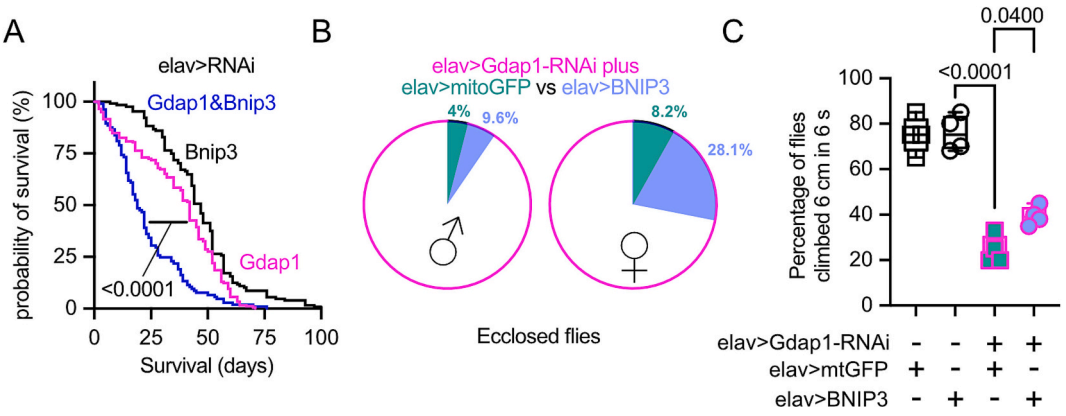

Fig. 5. BNIP3 protects against *Gdap1* depletion. (A) Lifespan of flies with neural-specific knockdown (KD) of *Gdap1* (*elav* > *Gdap1* RNAi, pink curve) and additional KD of *Bnip3* (*elav* > *Gdap1*-RNAi, *Bnip3*-RNAi, blue curve), compared to *Bnip3* KD flies alone (*elav* > *Bnip3*-RNAi, black curve). (B) Eclosion rate of Gdap1 KD flies expressing mito-GFP (green) as control) or Bnip3 (blue). Over 400 flies were scored for each sex. (C) Climbing ability assay of 30-day-old flies across four groups: elav>mtGFP (control, transparent squares), *elav* > *BNIP3* (*Bnip3* neural overexpression, circles), *elav* > *Gdap1*-RNAi, mtGFP (*Gdap1* neural KD, green-filled pink squares), and *elav* > *Gdap1*-RNAi, *Bnip3* (*Gdap1* neural KD with *Bnip3* overexpression, blue-filled pink circles). Each dot represents the mean value from a vial containing approximately 25 flies. Statistical tests and *p* values are indicated in the figure. Statistical significance was evaluated by the log-rank (Mantel-Cox) test in A, and one-way ANOVA followed by the Holm-Sidak multiple comparisons test in C. *P* values are indicated. (For interpretation of the references to colour in this figure legend, the reader is referred to the web version of this article.)

in mitophagy, cause CMT type 2 A (Züchner et al., 2004). Induced pluripotent stem cell (iPSC)-derived motoneurons (MNs) from CMT2A patients with mutant MFN2 exhibit a significant reduction in mitochondria accompanied by increased mitophagy (Rizzo et al., 2016).

Together, these findings suggest that the induction of mitophagy could be a promising target for clinical studies in CMT disease similar to other neurological disorders. Mitophagy stimulation through NAD+ supplementation, urolithin A, and actinonin effectively reversed memory impairment in both *Caenorhabditis elegans* and mouse models of Alzheimer's disease (Fang et al., 2019). In the nematode Aβ and tau models, these compounds reversed memory deficits through BNIP3/BNIP3L ortholog (DCT-1)-dependent pathways. In mouse models, mitophagy enhancement diminished amyloid plaques and prevented cognitive impairment through microglial phagocytosis and suppression of neuroinflammation, while also abolishing tau hyperphosphorylation in human neuronal cells (Fang et al., 2019). Particularly relevant to our work, these compounds significantly upregulated BNIP3L/NIX levels and activity, which was critical for their therapeutic effects (Fang et al., 2019). Notably, urolithin A has already been tested in humans and proven safe while improving mitochondrial health markers (Andreux et al., 2019). These mitophagy enhancers therefore warrant investigation in CMT4A models.

Our study also further validated Drosophila as a model for studying CMT4A pathogenesis. Neural-specific *Gdap1* knockdown impairs eclosion, climbing, and lifespan, demonstrating GDAP1's critical role in neuronal function. These phenotypes align with GDAP1's established functions in mitochondrial dynamics, redox balance, and metabolism (Niemann et al., 2005; Noack et al., 2012; Wolf et al., 2022). The conserved BNIP3 upregulation between human neuronal cells and Drosophila also underscores the evolutionary preservation of these pathways. This model thus enables detailed investigation of mitochondrial dysfunction in CMT4A and the evaluation of therapeutic approaches.

In conclusion, our study sheds light on the role of BNIP3-mediated mitophagy in the cellular response to *GDAP1* deficiency. We demonstrate that BNIP3 upregulation acts as a protective mechanism to mitigate the detrimental effects of *GDAP1* loss on mitochondrial function and neuronal survival. These findings not only advance our understanding of CMT4A pathogenesis but also highlight the potential of targeting mitophagy pathways as a therapeutic strategy for this devastating disorder. Further research into the precise molecular mechanisms linking *GDAP1* deficiency, mitochondrial dysfunction, and neurodegeneration will be crucial for developing effective treatments for CMT4A and related neurological disorders.

CRediT authorship contribution statement

Li Zhang: Writing – review & editing, Supervision, Investigation. **Alireza Pouya:** Investigation. **Janina Kopetzky:** Investigation. **Sara Bitar:** Investigation. **Christina Wolf:** Investigation. **Federica Dal Bello:** Investigation. **David Gomez-Zepeda:** Writing – original draft, Investigation, Formal analysis. **Stefan Tenzer:** Supervision, Formal analysis. **Axel Methner:** Writing – review & editing, Writing – original draft, Visualization, Supervision, Project administration, Funding acquisition, Formal analysis, Data curation, Conceptualization.

Declaration of generative AI and AI-assisted technologies in the writing process

During the preparation of this work the author used Claude in order to avoid orthographic or grammatical mistakes and to increase readability. After using this tool, the authors reviewed and edited the content as needed and take full responsibility for the content of the published article.

Declaration of competing interest

The authors declare that they have no conflict of interest.

Acknowledgment

This project was funded by the Deutsche Forschungsgemeinschaft grant number 517361457 to AM. The excellent support by the IMB Core Facility Microscopy is gratefully acknowledged. We want to thank Ruben Spohrer for his technical assistance with sample preparation for proteomics analysis and Sabine Arndt for proteomics data processing. We thank Marion Silies for providing lab space and support.

Data availability

The mass spectrometry proteomics data have been deposited to the ProteomeXchange Consortium(Vizcaíno et al., 2013) (https://proteomecentral.proteomexchange.org/) via the jPOSTrepo partner repository (Okuda et al., 2025) (https://repository.jpostdb.

org/) with the dataset identifiers PXD059922 for ProteomeXchange and JPST003536 for jPOSTrepo.

References

Andreux, P.A., Blanco-Bose, W., Ryu, D., Burdet, F., Ibberson, M., Aebischer, P., Auwerx, J., Singh, A., Rinsch, C., 2019. The mitophagy activator urolithin a is safe and induces a molecular signature of improved mitochondrial and cellular health in humans. Nat. Metab. 1, 595–603.

Barneo-Muñoz, M., Juárez, P., Civera-Tregón, A., Yndriago, L., Pla-Martin, D., Zenker, J., Cuevas-Martín, C., Estela, A., Sánchez-Aragó, M., Forteza-Vila, J., Cuezva, J.M., Chrast, R., Palau, F., 2015. Lack of GDAP1 induces neuronal calcium and mitochondrial defects in a knockout mouse model of charcot-marie-tooth neuropathy. PLoS Genet. 11, e1005115.

Baxter, R.V., Ben Othmane, K., Rochelle, J.M., Stajich, J.E., Hulette, C., Dew-Knight, S., Hentati, F., Ben Hamida, M., Bel, S., Stenger, J.E., Gilbert, J.R., Pericak-Vance, M.A., Vance, J.M., 2002. Ganglioside-induced differentiation-associated protein-1 is mutant in Charcot-Marie-tooth disease type 4A/8q21. Nat. Genet. 30, 21–22.

Cantarero, L., Juárez-Escoto, E., Civera-Tregón, A., Rodríguez-Sanz, M., Roldán, M., Benítez, R., Hoenicka, J., Palau, F., 2021. Mitochondria-lysosome membrane contacts are defective in GDAP1-related Charcot-Marie-tooth disease. Hum. Mol. Genet. 29, 3589–3605.

Chung, K.W., Kim, S.M., Sunwoo, I.N., Cho, S.Y., Hwang, S.J., Kim, J., Kang, S.H., Park, K.-D., Choi, K.-G., Choi, I.S., Choi, B.-O., 2008. A novel GDAP1 Q218E mutation in autosomal dominant Charcot-Marie-tooth disease. J. Hum. Genet. 53, 360–364.

Cuesta, A., Pedrola, L., Sevilla, T., García-Planells, J., Chumillas, M.J., Mayordomo, F., LeGuern, E., Marín, I., Vílchez, J.J., Palau, F., 2002. The gene encoding ganglioside-induced differentiation-associated protein 1 is mutated in axonal Charcot-Marie-tooth type 4A disease. Nat. Genet. 30, 22–25.

Debattisti, V., Scorrano, L., 2013. D. melanogaster, mitochondria and neurodegeneration: small model organism, big discoveries. Mol. Cell. Neurosci. 55, 77–86.

Distler, U., Kuharev, J., Navarro, P., Levin, Y., Schild, H., Tenzer, S., 2014. Drift time-specific collision energies enable deep-coverage data-independent acquisition proteomics. Nat. Methods 11, 167–170.

Fang, E.F., Hou, Y., Palikaras, K., Adriaanse, B.A., Kerr, J.S., Yang, B., Lautrup, S., Hasan-Olive, M.M., Caponio, D., Dan, X., Rocktäschel, P., Croteau, D.L., Akbari, M., Greig, N.H., Fladby, T., Nilsen, H., Cader, M.Z., Mattson, M.P., Tavernarakis, N., Bohr, V.A., 2019. Mitophagy inhibits amyloid-β and tau pathology and reverses cognitive deficits in models of Alzheimer's disease. Nat. Neurosci. 22, 401–412.

Field, J.T., Gordon, J.W., 2022. BNIP3 and nix: atypical regulators of cell fate. Biochim. Biophys. Acta, Mol. Cell Res. 1869, 119325.

Gang, H., Hai, Y., Dhingra, R., Gordon, J.W., Yurkova, N., Aviv, Y., Li, H., Aguilar, F., Marshall, A., Leygue, E., Kirshenbaum, L.A., 2011. A novel hypoxia-inducible spliced variant of mitochondrial death gene Bnip3 promotes survival of ventricular myocytes. Circ. Res. 108, 1084–1092.

Gang, H., Dhingra, R., Lin, J., Hai, Y., Aviv, Y., Margulets, V., Hamedani, M., Thanasupawat, T., Leygue, E., Klonisch, T., Davie, J.R., Kirshenbaum, L.A., 2015. PDK2-mediated alternative splicing switches Bnip3 from cell death to cell survival. J. Cell Biol. 210, 1101–1115.

Gleyzer, N., Vercauteren, K., Scarpulla, R.C., 2005. Control of mitochondrial transcription specificity factors (TFB1M and TFB2M) by nuclear respiratory factors (NRF-1 and NRF-2) and PGC-1 family coactivators. Mol. Cell. Biol. 25, 1354–1366.

Googins, M.R., Woghiren-Afegbua, A.O., Calderon, M., St Croix, C.M., Kiselyov, K.I., VanDemark, A.P., 2020. Structural and functional divergence of GDAP1 from the glutathione S-transferase superfamily. FASEB J. 34, 7192–7207.

Gutscher, M., Pauleau, A.-L., Marty, L., Brach, T., Wabnitz, G.H., Samstag, Y., Meyer, A. J., Dick, T.P., 2008. Real-time imaging of the intracellular glutathione redox potential. Nat. Methods 5, 553–559.

Huber, N., Guimaraes, S., Schrader, M., Suter, U., Niemann, A., 2013. Charcot-Marie-tooth disease-associated mutants of GDAP1 dissociate its roles in peroxisomal and mitochondrial fission. EMBO Rep. 14, 545–552.

Huber, N., Bieniossek, C., Wagner, K.M., Elsässer, H.-P., Suter, U., Berger, I., Niemann, A., 2016. Glutathione-conjugating and membrane-remodeling activity of GDAP1 relies on amphipathic C-terminal domain. Sci. Rep. 6, 36930.

Hughes, C.S., Foehr, S., Garfield, D.A., Furlong, E.E., Steinmetz, L.M., Krijgsveld, J., 2014. Ultrasensitive proteome analysis using paramagnetic bead technology. Mol. Syst. Biol. 10, 757.

Katayama, H., Kogure, T., Mizushima, N., Yoshimori, T., Miyawaki, A., 2011. A sensitive and quantitative technique for detecting autophagic events based on lysosomal delivery. Chem. Biol. 18, 1042–1052.

Kennerson, M.L., Yiu, E.M., Chuang, D.T., Kidambi, A., Tso, S.-C., Ly, C., Chaudhry, R., Drew, A.P., Rance, G., Delatycki, M.B., Züchner, S., Ryan, M.M., Nicholson, G.A., 2013. A new locus for X-linked dominant Charcot-Marie-tooth disease (CMTX6) is caused by mutations in the pyruvate dehydrogenase kinase isoenzyme 3 (PDK3) gene. Hum. Mol. Genet. 22, 1404–1416.

Laker, R.C., Xu, P., Ryall, K.A., Sujkowski, A., Kenwood, B.M., Chain, K.H., Zhang, M., Royal, M.A., Hoehn, K.L., Driscoll, M., Adler, P.N., Wessells, R.J., Saucerman, J.J., Yan, Z., 2014. A novel MitoTimer reporter gene for mitochondrial content, structure, stress, and damage in vivo. J. Biol. Chem. 289, 12005–12015.

Lieber, T., Jeedigunta, S.P., Palozzi, J.M., Lehmann, R., Hurd, T.R., 2019. Mitochondrial fragmentation drives selective removal of deleterious mtDNA in the germline. Nature 570, 380–384.

Litonin, D., Sologub, M., Shi, Y., Savkina, M., Anikin, M., Falkenberg, M., Gustafsson, C. M., Temiakov, D., 2010. Human mitochondrial transcription revisited. J. Biol. Chem. 285, 18129–18133.

López Del Amo, V., Seco-Cervera, M., García-Giménez, J.L., Whitworth, A.J., Pallardó, F. V., Galindo, M.I., 2015. Mitochondrial defects and neuromuscular degeneration caused by altered expression of Drosophila Gdap1: implications for the Charcot-Marie-tooth neuropathy. Hum. Mol. Genet. 24, 21–36.

López Del Amo, V., Palomino-Schätzlein, M., Seco-Cervera, M., García-Giménez, J.L., Pallardó, F.V., Pineda-Lucena, A., Galindo, M.I., 2017. A Drosophila model of GDAP1 function reveals the involvement of insulin signalling in the mitochondria-dependent neuromuscular degeneration. Biochim. Biophys. Acta Mol. basis Dis. 1863, 801–809.

Mazure, N.M., Pouysségur, J., 2009. Atypical BH3-domains of BNIP3 and BNIP3L lead to autophagy in hypoxia. Autophagy 5, 868–869.

Metukuri, M.R., Beer-Stolz, D., Namas, R.A., Dhupar, R., Torres, A., Loughran, P.A., Jefferson, B.S., Tsung, A., Billiar, T.R., Vodovotz, Y., Zamora, R., 2009. Expression and subcellular localization of BNIP3 in hypoxic hepatocytes and liver stress. Am. J. Physiol. Gastrointest. Liver Physiol. 296, G499–G509.

Niemann, A., Ruegg, M., La Padula, V., Schenone, A., Suter, U., 2005. Ganglioside-induced differentiation associated protein 1 is a regulator of the mitochondrial network: new implications for Charcot-Marie-tooth disease. J. Cell Biol. 170, 1067–1078.

Niemann, A., Wagner, K.M., Ruegg, M., Suter, U., 2009. GDAP1 mutations differ in their effects on mitochondrial dynamics and apoptosis depending on the mode of inheritance. Neurobiol. Dis. 36, 509–520.

Niemann, A., Huber, N., Wagner, K.M., Somandin, C., Horn, M., Lebrun-Julien, F., Angst, B., Pereira, J.A., Halfter, H., Welzl, H., Feltri, M.L., Wrabetz, L., Young, P., Wessig, C., Toyka, K.V., Suter, U., 2014. The Gdap1 knockout mouse mechanistically links redox control to Charcot-Marie-tooth disease. Brain 137, 668–682.

Noack, R., Frede, S., Albrecht, P., Henke, N., Pfeiffer, A., Knoll, K., Dehmel, T., Hörste G., Meyer Zu, Stettner, M., Kieseier, B.C., Summer, H., Golz, S., Kochanski, A., Wiedau-Pazos, M., Arnold, S., Lewerenz, J., Methner, A., 2012. Charcot-Marie-tooth disease CMT4A: GDAP1 increases cellular glutathione and the mitochondrial membrane potential. Hum. Mol. Genet. 21, 150–162.

Okuda, S., Yoshizawa, A.C., Kobayashi, D., Takahashi, Y., Watanabe, Y., Moriya, Y., Hatano, A., Takami, T., Matsumoto, M., Araki, N., Tabata, T., Iwasaki, M., Sugiyama, N., Kodera, Y., Tanaka, S., Goto, S., Kawano, S., Ishihama, Y., 2025. jPOST environment accelerates the reuse and reanalysis of public proteome mass spectrometry data. Nucleic Acids Res. 53, D462–D467.

Pedrola, L., Espert, A., Wu, X., Claramunt, R., Shy, M.E., Palau, F., 2005. GDAP1, the protein causing Charcot-Marie-tooth disease type 4A, is expressed in neurons and is associated with mitochondria. Hum. Mol. Genet. 14, 1087–1094.

Pijuan, J., Cantarero, L., Natera-de Benito, D., Altimir, A., Altisent-Huguet, A., Díaz-Osorio, Y., Carrera-García, L., Expósito-Escudero, J., Ortez, C., Nascimento, A., Hoenicka, J., Palau, F., 2022. Mitochondrial dynamics and mitochondria-lysosome contacts in neurogenetic diseases. Front. Neurosci. 16, 784880.

Pla-Martín, D., Rueda, C.B., Estela, A., Sánchez-Piris, M., González-Sánchez, P., Traba, J., de la Fuente, S., Scorrano, L., Renau-Piqueras, J., Alvarez, J., Satrústegui, J., Palau, F., 2013. Silencing of the Charcot-Marie-tooth disease-associated gene GDAP1 induces abnormal mitochondrial distribution and affects Ca2+ homeostasis by reducing store-operated Ca2+ entry. Neurobiol. Dis. 55, 140–151.

Rizzo, F., Ronchi, D., Salani, S., Nizzardo, M., Fortunato, F., Bordoni, A., Stuppia, G., Del Bo, R., Piga, D., Fato, R., Bresolin, N., Comi, G.P., Corti, S., 2016. Selective mitochondrial depletion, apoptosis resistance, and increased mitophagy in human Charcot-Marie-tooth 2A motor neurons. Hum. Mol. Genet. 25, 4266–4281.

Schmid, E.T., Pyo, J.-H., Walker, D.W., 2022. Neuronal induction of BNIP3-mediated mitophagy slows systemic aging in Drosophila. Nat. Aging 2, 494–507.

Senderek, J., Bergmann, C., Ramaekers, V.T., Nelis, E., Bernert, G., Makowski, A., Züchner, S., De Jonghe, P., Rudnik-Schöneborn, S., Zerres, K., Schröder, J.M., 2003. Mutations in the ganglioside-induced differentiation-associated protein-1 (GDAP1) gene in intermediate type autosomal recessive Charcot-Marie-tooth neuropathy. Brain 126, 642–649.

Shield, A.J., Murray, T.P., Board, P.G., 2006. Functional characterisation of ganglioside-induced differentiation-associated protein 1 as a glutathione transferase. Biochem. Biophys. Res. Commun. 347, 859–866.

Sielaff, M., Kuharev, J., Bohn, T., Hahlbrock, J., Bopp, T., Tenzer, S., Distler, U., 2017. Evaluation of FASP, SP3, and iST protocols for proteomic sample preparation in the low microgram range. J. Proteome Res. 16, 4060–4072.

Szklarczyk, D., Gable, A.L., Nastou, K.C., Lyon, D., Kirsch, R., Pyysalo, S., Doncheva, N. T., Legeay, M., Fang, T., Bork, P., Jensen, L.J., von Mering, C., 2020. The STRING database in 2021: customizable protein–protein networks, and functional characterization of user-uploaded gene/measurement sets. Nucleic Acids Res. 49, D605–D612.

Vargas, J.N.S., Hamasaki, M., Kawabata, T., Youle, R.J., Yoshimori, T., 2023. The mechanisms and roles of selective autophagy in mammals. Nat. Rev. Mol. Cell Biol. 24, 167–185.

Vizcaíno, J.A., Côté, R.G., Csordas, A., Dianes, J.A., Fabregat, A., Foster, J.M., Griss, J., Alpi, E., Birim, M., Contell, J., O'Kelly, G., Schoenegger, A., Ovelleiro, D., Pérez-Riverol, Y., Reisinger, F., Ríos, D., Wang, R., Hermjakob, H., 2013. The PRoteomics IDEntifications (PRIDE) database and associated tools: status in 2013. Nucleic Acids Res. 41, D1063–D1069.

Wieckowski, M.R., Giorgi, C., Lebiedzinska, M., Duszynski, J., Pinton, P., 2009. Isolation of mitochondria-associated membranes and mitochondria from animal tissues and cells. Nat. Protoc. 4, 1582–1590.

Wolf, C., Pouya, A., Bitar, S., Pfeiffer, A., Bueno, D., Rojas-Charry, L., Arndt, S., Gomez-Zepeda, D., Tenzer, S., Bello, F.D., Vianello, C., Ritz, S., Schwirz, J., Dobrindt, K.,

Peitz, M., Hanschmann, E.-M., Mencke, P., Boussaad, I., Silies, M., Brüstle, O., Giacomello, M., Krüger, R., Methner, A., 2022. GDAP1 loss of function inhibits the mitochondrial pyruvate dehydrogenase complex by altering the actin cytoskeleton. Commun. Biol. 5, 541.

Zhang, J., Ney, P.A., 2009. Role of BNIP3 and NIX in cell death, autophagy, and mitophagy. Cell Death Differ. 16, 939–946.

Zhang, T., Xue, L., Li, L., Tang, C., Wan, Z., Wang, R., Tan, J., Tan, Y., Han, H., Tian, R., Billiar, T.R., Tao, W.A., Zhang, Z., 2016. BNIP3 protein suppresses PINK1 kinase proteolytic cleavage to promote mitophagy. J. Biol. Chem. 291, 21616–21629.

Züchner, S., Mersiyanova, I.V., Muglia, M., Bissar-Tadmouri, N., Rochelle, J., Dadali, E. L., Zappia, M., Nelis, E., Patitucci, A., Senderek, J., Parman, Y., Evgrafov, O., Jonghe, P.D., Takahashi, Y., Tsuji, S., Pericak-Vance, M.A., Quattrone, A., Battologlu, E., Polyakov, A.V., Timmerman, V., Schröder, J.M., Vance, J.M., 2004. Corrigendum: mutations in the mitochondrial GTPase mitofusin 2 cause Charcot-Marie-tooth neuropathy type 2A. Nat. Genet. 36, 449–451. https://doi.org/10.1038/ng1341.